Predicting Long-Term Hydrological Change Caused By Climate Shifting In The 21st Century In The Headwater Area of The Yellow River Basin

Jingyi Hu (2269722132@qq.com)
Xi'an Jiaotong University https://orcid.org/0000-0001-5212-0440
Yiping Wu
Xi'an Jiaotong University https://orcid.org/0000-0002-5163-0884
Pengcheng Sun
Xi'an Jiaotong University
Fubo Zhao
Xi'an Jiaotong University
Ke Sun
Xi'an Jiaotong University
Tiejian Li
Tsinghua University
Bellie Sivakumar
Indian Institute of Technology Bombay
Linjing Qiu
Xi'an Jiaotong University
Yuzhu Sun
Xi'an Jiaotong University
Zhangdong Jin
Chinese Academy of Sciences Institute of Earth Environment

Research Article

Keywords: Climate change, Hydrological components, Representative Concentration Pathways, SWAT

Posted Date: July 15th, 2021

DOI: https://doi.org/10.21203/rs.3.rs-696446/v1

Predicting long-term hydrological change caused by climate shifting in the 21st Century in the headwater area of the Yellow River Basin

Jingyi Hu[1], Yiping Wu[1,*], Pengcheng Sun[1], Fubo Zhao[1], Ke Sun[1], Tiejian Li[2], Bellie Sivakumar[3], Linjing Qiu[1], Yuzhu Sun[1] and Zhangdong Jin[4,5,1]

[1] Department of Earth & Environmental Science, Xi'an Jiaotong University, Xi'an, Shaanxi Province, 710049, China

[2] State Key Laboratory of Hydroscience and Engineering, Tsinghua University, Beijing, 100084, China

[3] Department of Civil Engineering, Indian Institute of Technology Bombay, Powai, Mumbai, 400076, India

[4] SKLLQG, Institute of Earth Environment, Chinese Academy of Sciences, Xi'an, 710075, China

[5] CAS Center for Excellence in Quaternary Science and Global Change, Xi'an, 710061, China

* Corresponding author (rocky.ypwu@gmail.com)

Content List

Abstract

The Qinghai-Tibetan Plateau (QTP) is one of the amplifiers of global climate change. The headwater area of the Yellow River Basin (HYRB) on the QTP is the dominant water source region for the whole Yellow River Basin (YRB). However, the sensitive responses of hydrological processes to the intensifying climate change are exerting high uncertainties to the water cycle in the HYRB. The aim of this study was to investigate the potential climate change under three Representative Concentration Pathways (RCP 2.6, 4.5, and 8.5) and their hydrological impacts in this region using the ensemble climate data from eight general circulation models (GCMs) and the Soil and Water Assessment Tool (SWAT). Compared to the baseline (1976–2015), the projected climate indicated a rise of 7.3–7.8% in annual precipitation, 1.3–1.9°C in maximum air temperature, and 1.2–1.8°C in minimum air temperature during the near future period (2020–2059), and an increment of 9.0–17.9%, 1.5–4.5°C, and 1.3–4.5°C in precipitation, maximum and minimum temperature, respectively, during the far future period (2060–2099). The well-simulated SWAT modeling results suggested that due to a wetter and warmer climate, annual average actual evapotranspiration (AET) would increase obviously in the future (31.9–35.3% during the near future and 33.5–54.3% during the far future), which might cause a slight decrease in soil water. Water yield would decrease by 16.5–20.1% during the near future period, implying a worsening water crisis in the future. Till the end of this century, driven by the increased precipitation, water yield would no longer continue to decrease, with a decline by 15–19.5%. Overall, this study can not only provide scientific understanding of the

hydrological responses to the future climate in both semi-arid and alpine areas, but also contribute to the decision support for sustainable development of water resources and protection of eco-environment in the HYRB.

Keywords: Climate change; Hydrological components; Representative Concentration Pathways; SWAT

1 Introduction

Global warming is one of the most important threats to human society. Indeed, it has already begun to threaten the sustainability of Earth's life support systems (Lubchenco, 1998). According to Intergovernmental Panel on Climate Change (IPCC) reports, the global average air temperature has increased by 0.85 °C from 1880 to 2012, and the situation might get worse as temperature are anticipated to rise by 1–5 °C by the end of the 21st century (Holden *et al.*, 2018; Lin *et al.*, 2018; Stocker *et al.*, 2013). Recent studies have pointed out that high-altitude regions, such as the Qinghai-Tibetan Plateau (QTP), were the amplifier of global climate change (Giorgi *et al.*, 2010; Jian *et al.*, 2014; Liu and Chen, 2015). Due to the high altitude, low temperature, and slow vegetation growth, the ecosystems in these regions are fragile and difficult to be repaired once damaged (Wang *et al.*, 2007). Thus, these regions are experiencing much more changes and uncertainties caused by the global climate change than other regions.

Global warming could affect the water resources and complicate their assessment and management (Christensen *et al.*, 2004; Oki and Kanae, 2006; Zhou *et al.*, 2011). The increase of temperature has made the spatial and temporal variability of

92 precipitation increase, which caused more frequent drought and flood events and more
93 serious economic losses (Piao *et al.*, 2010; Trenberth *et al.*, 2014). Associated with
94 global warming, the actual evapotranspiration (AET) has also changed significantly
95 during the past several decades, resulting in the loss of soil water and runoff (Berg *et*
96 *al.*, 2017; Donnelly *et al.*, 2017). Coles *et al.* (2017) assessed trends in climatological
97 and hydrological variables of hillslopes on Great Plains, and found that snowmelt-
98 runoff and spring soil water content all decreased. In the future, a warming climate
99 would accelerate multiphase water transformation processes and increase the
100 uncertainty of water cycle prediction, preventing us from making firm statements
101 (Meaurio *et al.*, 2017; Wu *et al.*, 2016; Zhang *et al.*, 2016). Liu *et al.* (2017) examined
102 the impacts of 1.5 and 2 °C global warming on water cycle and indicated drier springs,
103 and more severe floods over long return periods (25 and 50 years) for Yiluo and
104 Beijiang River catchment.Yang *et al.* (2014) reported that the weakened water vapor
105 exchange led to less precipitation in the monsoon-impacted southern and eastern
106 Plateau, but the warming enhanced land evaporation. An in-depth understanding of the
107 future climate change impacts on water cycles is hence of great significance for the
108 water resource management and associated policy formulation, which has also been an
109 important concern in the field of global change studies.

110 Various methods have been proposed and utilized to disentangle climate change
111 impacts on watershed hydrology (Zhang *et al.*, 2018), such as paired catchment
112 approach, hydrological modelling approach, conceptual approach, empirically
113 statistical method, and hydrological sensitivity method (Gao *et al.*, 2016; Zhang *et al.*,

2017). Because hydrological models relate model parameters directly to physically observable land surface characteristics, this method can effectively extract a significant amount of information from limited existing data (Yang *et al.*, 2017). Lu *et al.* (2018) used Variable Infiltration Capacity (VIC) model and RegCM4 and found that evapotranspiration would increase by 10–60% in the source regions of Yellow and Yangtze rivers due to the temperature rise. Recently, a common approach for assessing future hydrological conditions is to use General Circulation Model (GCM) projections in combination with hydrological models (Chen *et al.*, 2012). The Soil and Water Assessment Tool (SWAT), a physical-based, semi-distributed, and bio-physical model, is suitable to investigate the response of simulated streamflow to climate change, especially with the help of projected climate data from various GCMs (Arnold *et al.*, 1998; Zhao *et al.*, 2018). For example, using SWAT and outputs from 20 GCMs to estimate the potential hydrological changes, Neupane *et al.* (2019) found that the mean annual streamflow would decrease under the worst-case Representative Concentration Pathways (RCP) 8.5 during the 2080s in the Suwannee River Basin in the United States.

The headwater area of the Yellow River Basin (HYRB) on the QTP is the source region of the Yellow River, the second largest river in China. The HYRB is crucial to the Yellow River Basin (YRB), as it contributed nearly 40% water to the whole YRB with an area of only about 16% (Chu *et al.*, 2018). It was reported that the HYRB is one of the high-altitude regions with the richest biodiversity in the world (Guo *et al.*, 2004). Therefore, the specific ecosystem in this region is valuable and critical for the YRB, and even for the whole globe. The unique geographical location and climate

conditions make the ecosystem of the HYRB fragile and sensitive to environmental changes (Sun *et al.*, 2019; Zhang *et al.*, 2013; Zhou *et al.*, 2005). In the context of global climate change, the HYRB is experiencing a much more intense climate change and associated effects, thus greatly increasing the uncertainties of water resources in this region. The annual average flow of the HYRB has decreased over the past 50 years (Cuo *et al.*, 2013). What is worse, the runoff in the 1990s suffered a serious decrease and the zero-flow days at the most upstream gauging station (Huangheyan station) increased (Chen *et al.*, 2007; Hu *et al.*, 2011; Zhang *et al.*, 2004), which, in long term, could influence the ecological environment and socio-economic development in the HYRB (Lin *et al.*, 2012). Besides, due to the characteristics of water shortage in semi-arid areas, comprehensive research including climate and hydrology needs to be used to evaluate possible strategies in order to make these areas less affected by the changing climate (Patel *et al.*, 2020).Thus, accurately assessing the potential impacts of climate change on the key hydrological processes in the HYRB is an urgent and important task for water resources management.

Our modeling result will provide a proper perspective for investigating the main influencing climate factors of the hydrological components, which is not only useful for people to formulate suitable strategies and policies in semi-arid area, but also key to the sustainable development of the eco-environment in the YRB. With this in mind, the goal of the present study was to assess the hydrological responses to the future projected climate in the HYRB during the near-future period (2020–2059) and far-future period (2060–2099). The assessment was made for three RCP scenarios (RCP

158 2.6, 4.5, and 8.5) using an ensemble of eight downscaled GCMs and SWAT modeling.
159 The specific objectives were: (1) to validate the suitability and performance of the
160 SWAT model in simulating the hydrological processes in the HYRB; (2) to predict the
161 characteristics of air temperature and precipitation from CMIP5 GCMs under the above
162 three scenarios; and (3) to investigate the spatiotemporal patterns of the key
163 hydrological components (including AET, soil water, and water yield) over the whole
164 basin and across the 21st Century. The outcomes of this study are anticipated to provide
165 a good scientific basis for the sustainable management of the HYRB.
166

167 ## 2 Materials and methods

168 ### 2.1 Study area

169 The HYRB, well known as the 'water tower' of the Yellow River basin, is located in
170 the Qinghai Province and the northeastern part of the QTP with an area of 118,000 km^2,
171 accounting for 16.2% of the YRB (Figure 1). The average annual precipitation (based
172 on observations over the period 1956–2015) is approximately 497 mm and the average
173 annual temperature is about 1.8°C. The average annual runoff (based on observations
174 over the period 1956–2012) is 19,800,000,000 m^3, which is as much as about 42% of
175 the runoff of the Yellow River Basin in the corresponding period. In comparison with
176 the middle and lower reaches, the upper reach of the HYRB is less affected by
177 anthropogenic activities. So, the response of hydrological components to climate
178 change could be reflected objectively in the HYRB.
179

2.2 Model description

The SWAT model was developed by the United States Department of Agriculture, Agricultural Research Service (USDA-ARS), and has been widely used to predict the impact of climate change and land use change on water, sediment, and chemical components (Arnold *et al.*, 1998). The hydrological components in the SWAT is based on the water balance equation (Gassman *et al.*, 2007):

$$SW_t = SW + \sum_{i=1}^{t}(R_i - Q_i - ET_i - P_i - QR_i) \quad (1)$$

where SW is the soil water content, i is the time t (days) for the simulation period, R (mm), Q (mm), ET (mm), P (mm), and QR (mm) are the daily amounts of precipitation, runoff, evapotranspiration, percolation, and return flow, respectively. Hydrological Response Unit (HRU) is the basic unit in SWAT. The HRU is defined as a unique aggregation of land use, soil properties, management, and terrain slope (Flügel, 2010; Patel and Srivastava, 2013). In the modeling process, we facilitated the elevation band to discretize the topographic effects of temperature and precipitation into snow melting and runoff (Hartman *et al.*, 1999).

2.3 Model input data

The monthly streamflow data observed over the period 1970–2010 at the Tangnaihai gaging station were provided by the Yellow River Conservancy Commission of the Ministry of Water Resources (http://www.yrcc.gov.cn/). Meteorological data observed over the period 1951–2015 at 16 stations, including daily maximum temperature (TMAX), minimum temperature (TMIN), precipitation, wind speed, solar radiation,

and relative humidity, were provided by the Data Center of the China Meteorological Administration (CMA, http://data.cma.cn/). The input data also included digital elevation model (DEM), soil type, and land use. The 90 m × 90 m Shuttle Radar Topography Mission (SRTM) DEM were used to extract the flow direction and accumulation, create streams, delineate the watershed, and calculate the subbasin parameters. Land use data of the year 1980 (1 km × 1 km) and soil data with a 1:1 million scale were provided by the Ecological and Environmental Science Data Center for West China (http://westdc.westgis.ac.cn). Land use data were reclassified into seven major classes including mid-density and sparse grassland (56.9%), dense grassland (19.0%), barren or sparsely vegetated land (14.4%), forest (7.3%), water bodies (2.8%), cropland (0.4%) and urban, industrial and residential land (0.03%).

2.4 Model setup, calibration, and validation

The HYRB was divided into 157 subbasins based on DEM and digital stream network information, and the subbasins were further divided into 2205 HRUs using a threshold of 5% for each of land use, soil class, and slope. The monthly streamflow data from the Tangnaihai gauging station at the watershed outlet was used to calibrate and validate the SWAT model. In this study, SWAT-CUP (Calibration and Uncertainty Procedures) was used to identify the set of parameters based on the sensitivity analysis and generate the optimized values of the parameters (Abbaspour *et al.*, 2007; Andrianaki *et al.*, 2019; Xu *et al.*, 2009) (listed in Table 2). The Sequential Uncertainty Fitting version 2 (SUFI-2) algorithm was adopted for the parameter optimization in this

223 study (Yang *et al.*, 2008). The monthly streamflow data were available for 40 years
224 (1971–2010), from which a twenty-year (1981–2000) record of monthly streamflow
225 was used to calibrate the model, and the other twenty-year (1971–1980 and 2001–2010)
226 record was used for validation. We used a series of numeric criteria to evaluate the
227 model performance, including the Nash-Sutcliffe efficiency (NSE), coefficient of
228 determination (R^2), and percentage bias (PBIAS). Details of these are presented in
229 Appendix 1.

230 2.5 Future climate scenarios

231 In this study, eight General Circulation Models (GCMs) were selected for climate
232 change projections. The data were downloaded from the ESGF's website
233 (http://pcmdi9.llnl.gov/). Details of the data sources used in this study are presented in
234 Table 1. The daily data sets (precipitation, maximum and minimum temperatures) of
235 the above three GCMs were selected under RCP 2.6, 4.5, and 8.5 scenarios
236 (representing a very low forcing scenario, medium stabilization scenario, and very high
237 emission scenario, respectively) to predict the future climate scenarios. Two future
238 periods were considered to study the temporal change of hydrological components: near
239 future: 2020–2059 and far future: 2060–2099. The impacts of climate change on
240 hydrological components were investigated by comparing the yearly and monthly
241 difference between the baseline (1976–2015) and the future projections from the model
242 outputs. Specifically, we used absolute changes to evaluate future maximum and
243 minimum temperature, and relative changes to evaluate future precipitation, AET, soil
244 water, and water yield.

Before implementing the GCM output data in SWAT modeling, it is necessary to downscale the raw data to get a fine resolution (Wilby *et al.*, 2002). In this study, we used bilinear interpolation to obtain high-resolution data that could be used in hydrological models (Bae *et al.*, 2015; Sun *et al.*, 2016); see Appendix 2 and Figure S2 for details. Then we used a simple bias correction method to correct the downscaled data. The correction of precipitation used the relative change between the monthly observed and simulated data of the historical period (1971–1990), while temperature used the monthly absolute change for the historical period. These biased climate data were calculated as follows:

$$P_{fm} = (1 + \alpha_m) \times P_{fm0} \tag{2}$$

$$\alpha_m = \frac{P_{hm} - P_{hm0}}{P_{hm0}} \tag{3}$$

$$T_{fm} = \beta_m + T_{fm0} \tag{4}$$

$$\beta_m = T_{hm} - T_{hm0} \tag{5}$$

where m is the month m, P_{fm} and T_{fm} are the corrected GCMs precipitation and temperature, P_{fm0} and T_{fm0} are initial GCMs precipitation and temperature, P_{hm} and T_{hm} are GCMs precipitation and temperature data in historical period, P_{hm0} and T_{fm0} are CMA precipitation and temperature data.

The GCMs data were evaluated by comparing with the CMA data during the historical period (1986–2005) (Figure S3). Although the downscaling procedure for precipitation underestimated some peaks, the downscaled data were generally consistent with the CMA-based observations, with R^2 being 0.87 (Figure S3a). For the monthly maximum and minimum temperatures, the downscaled data were in much

closer agreement with the observed data than the case for monthly precipitation, as shown in Figure S3b and c. The R^2 between monthly temperature (maximum and minimum) derived from the downscaled GCMs and CMA exceeded 0.95 (0.96 for maximum and 0.98 for minimum). Generally, both the simulated downscaled precipitation and the temperature values were in close agreement with the observed ones, suggesting that the real climate conditions of the study area (HYRB) could be fairly accurately reflected by the downscaled climate data derived from the GCMs.

2.6 Statistical analysis

In this study, the unitary linearity regress method was used to fit the relation between variables. The prediction model of the univariate linear regression analysis method is as follows:

$$Y_t = ax_t + b \tag{6}$$

$$\mathrm{b} = \frac{\sum Y_i}{n} - a\frac{\sum x_i}{n} \tag{7}$$

$$\mathrm{a} = \frac{n\sum x_i Y_i - \sum x_i \sum Y_i}{n\sum x_i^2 - (\sum x_i)^2} \tag{8}$$

where x_t represents the value of independent variable in t period, Y_t represents the value of dependent variable in t period, a and b represent the parameter of linear regression equation.

We also used Mann-Kendall nonparametric rank test to analyze the trend of hydrological and meteorological elements (Kendall and MauriceG, 1979). The rank correlation test for two sets of observations $\mathrm{X} = x_1, x_2, \ldots x_n$ and $\mathrm{Y} = y_1, y_2, \ldots y_n$ is

281 formulated as follows. The statistic S is calculated as follows:

$$S = \sum_{i<j} a_{ij}\, b_{ij} \tag{9}$$

282 where

$$a_{ij} = sgn(x_j - x_i) = \begin{cases} 1 & x_i < x_j \\ 0 & x_i = x_j \\ -1 & x_i > x_j \end{cases} \tag{10}$$

283 and b_{ij} is similarly defined for the observations in Y. Under the null hypothesis that X
284 and Y are independent and randomly ordered, the statistic S tends to normality for large
285 n, with $E(S) = 0$ and variance given by:

$$var(S) = \frac{n(n-1)(2n+5)}{10} \tag{11}$$

286 The significance of trends is tested by comparing the standardized test statistic Z with
287 the standard normal variate at the desired significance level. Z is calculated as:

$$Z = \begin{cases} \dfrac{(S-1)}{\sqrt{var(S)}} & S > 0 \\ 0 & S = 0 \\ \dfrac{(S+1)}{\sqrt{var(S)}} & S < 0 \end{cases} \tag{12}$$

288 $|Z| \geq 1.64$ means that the confidence level in the current test is more than 95%
289 ($p<0.05$).

290

291 **3 Results**

292 3.1 Model evaluation

293 A visual comparison of the monthly simulated streamflow values against the monthly
294 observed streamflow values for the calibration (1981–2000) and validation (1971–1980
295 and 2001–2010) periods is shown in Figure 2. Although there were three peak flows

296 (e.g., 1981, 1983, and 1999) underestimated and two peak flows (e.g. 1995 and 2007)
297 overestimated during extreme high-water years, the monthly streamflow simulations
298 generally matched well with the observations. The results from the statistical evaluation
299 were presented in Table 3. For the calibration period, the model performed efficiently
300 with the NSE of 0.85, R^2 of 0.86, and PBIAS of -0.3%. As for the validation periods,
301 the NSEs were 0.87 and 0.82, R^2 were 0.88 and 0.89, and PBIAS were -0.3% and 11.3%
302 for validation period I (1971–1980) and validation period II (2001–2010), respectively.
303 Based on the performance ratings of assuming typical uncertainty in observations given
304 by Pereira *et al.* (2016), the streamflow simulation in this study could be evaluated as
305 'good' ($|PBIAS| \leq 15\%$, $0.8 \leq NSE$, and $R^2 \geq 0.85$). These results indicate that the
306 SWAT model performed well in the HYRB and can be used to investigate the future
307 climate change impacts on hydrological processes.
308
309 3.2 Historical spatiotemporal characteristics of key hydrological components
310 Figure 3 showed that the average annual AET was about 292 mm during 1976–2015,
311 with a range of 250 mm in 1997 to 329 mm in 2012. SD (standard deviation) of AET
312 was 19.46 mm, which means AET fluctuated greatly during the study period. The linear
313 fitting results showed that AET in the whole region increased significantly with a rate
314 of 0.93 mm/yr, which was due to the increase of precipitation and temperature in this
315 region (Figure S1). Spatially, in comparison with the northwestern part, the
316 southeastern part of the basin had a higher AET value (Figure 4 a). From 1976 to 2015,
317 AET increased mainly in the southeast, central and western parts of the basin, and the

318 change in most areas is significant. While it decreased slightly in the northeast (Figure
319 4 d and g). Table 4 showed that 84.2% of the basin experienced increased AET with a
320 rate ranging from 0.1 to 2.0 mm/yr, with significant increasing portion detected for
321 74.0%.

322 The basin-average soil water approximately amounted to 120 mm during 1976–2015
323 (Figure 3). During the study period, the minimum soil water was 116 mm, which
324 appeared in 1988, and the maximum value was 126 mm, which appeared in 1983. Soil
325 water in the whole region showed a slightly decreasing trend with a rate of 0.05 mm/yr
326 during the 40-year period. Soil water showed an increasing gradient from the northwest
327 to the southeast with a range of 0 to 578 mm (Figure 4 b). There was abundant rainfall
328 and high coverage grassland in the southeast, which could increase the retention time
329 of rainwater on the land surface and increase the infiltration of rainwater, so the soil
330 water in this area was higher. Figure 4 h showed that the area with decreased soil water
331 was greater than the increased one, and we could also find the same result from Table
332 4.

333 Water yield refers to the capacity of a catchment to supply water (Arnold *et al.*, 1998).
334 The average water yield in study area was 205 mm with a range of 147 to 305 mm
335 during 1976–2015 (Figure 3). The SD of water yield was 35.65 mm, and the linear
336 fitting results showed that the water yield decreased by 0.02 mm/yr, and the downward
337 trend was insignificant. From Figure 4 c, we found that water yield of the basin had
338 obvious spatial heterogeneity, that is, water yield of the eastern and southern region was
339 much higher than that in the western and northern area. During the study period, water

yield mainly showed a decreasing trend in the south of basin (about 51.8% of the whole basin), while the western and northern regions showed an increasing trend (48.2% of the whole basin) (Figure 4 i and Table 4). Besides, there was no statistical significance in the trend of water yield in both increasing and decreasing areas.

3.3 Projected climate over the 21st century

The downscaled data were analyzed for the two future time periods: near future (2020–2059) and far future (2060–2099). The future bias-corrected scenarios RCP 2.6, RCP 4.5, and RCP 8.5 were then compared with the observed climate data from the historical period (1976–2015).

Figure 5 showed that during the near future period, the annual increases in precipitation were found to be 7.3%, 7.6%, and 7.8% under RCP 2.6, RCP 4.5, and RCP 8.5, respectively. The annual precipitation was projected to continuously increase in the HYRB under three RCPs during the far future period. From the Table 5, we found that the CV (coefficient of variation) of far future period precipitation was higher than that of near future period precipitation. Figure 6 (a) showed that the precipitation in the HYRB mainly concentrated from May to September every year during the historical period. The rainfall in the study area would increase in every month, while the changes in monthly projected rainfall showed large differences (Figure 6 b). The precipitation increased most obviously in January and November. In particular, it was anticipated to increase by 63% and 63.3% in these two months under RCP 8.5 scenario during the far future period. These results indicated that the future precipitation changes had temporal

362 heterogeneity under different scenarios.

363 Both annual and monthly temperatures showed a significant warming trend across
364 the HYRB (Figure 5 and Figure 6). Under RCP 2.6, the increment of temperature was
365 similar during the near future and far future periods. Under RCP 4.5 scenario, the
366 maximum temperature increased by 1.6 °C and the minimum temperature increased by
367 1.5 °C in the near future period. The maximum temperature and minimum temperature
368 increased by 2.6 °C and 2.4 °C respectively in the far future period. The HYRB was
369 projected to experience the warmest period at the end of this century under RCP 8.5, in
370 which period the maximum temperature and minimum temperature were expected to
371 increase by 4.5 °C. Table 5 indicated that the CV of far future period temperature was
372 higher than that of near future period temperature. Figure 6 (a) showed that the
373 maximum values of the maximum and minimum temperature in the HYRB appear in
374 July and the minimum values appear in January. The maximum temperature increased
375 the most in October (by 5.2 °C), and the minimum temperature increased the most in
376 March (by 6.4 °C), which occurred in the RCP 8.5 scenario at the end of this century
377 (Figure 6 c and d).

378

379 3.4 Hydrological responses to projected climate change

380 We analyzed the effects of climate change on several key hydrological components
381 in the HYRB, including actual evapotranspiration (AET), soil water, and water yield.
382 Figure 7 and Figure 8 showed the annual and monthly change, respectively, of the future
383 AET, soil water, and water yield.

Figure 7 indicated that AET was sensitive to climate change. During the near future period, the increment of AET in the three RCPs was similar, ranging from 31.9% to 35.3%. During the far future period, AET continued to increase, with the most dramatic increase under RCP 8.5 scenario, which might be related to obvious increase of precipitation and temperature in the HYRB. From the Figure 8 (a), we found that the AET in historical period reached its maximum in July. During the near future and far future period, AET showed an increasing trend (Figure 8 b). AET was projected to increase greatly in March, April, October, and November, and the maximum increment occurred under RCP 8.5 scenario at the end of this century, with a change rate of 174%. Figure S4 showed the spatial changes of AET compared with historical periods. The AET of the whole basin would increase in the future, while it increased more obviously in the eastern and southern part of the basin, indicating more water loss in this region in the future. Compared with RCP 2.6 and RCP 4.5, AET increased most under RCP 8.5, which was related to the different temperature changes under the three scenarios.

Soil water decreased slightly during near future period, by 3.1% in RCP 2.6 scenario, 6.1% in RCP 4.5, and 8.5 scenarios (Figure 7). By the end of this century, soil water decreased more obviously, by 13.3% under RCP 8.5 scenario compared with base period, which could affect the absorption of water by vegetation The monthly variation of soil water was shown in Figure 8 (c). Under different scenarios, soil water decreased most obviously in April and May. The change of soil water was similar to that of temperature, which meant that although the rainfall increased in this region, the increase of ET due to raise of temperature played a greater role. Figure S5 showed that the

406 decrease of soil water was predicted to be mainly in the west, middle and export areas
407 of the basin, while it would increase slightly in the southeastern region. Compared with
408 the near future period, the increment of soil water in southeast may decrease during the
409 far future period, and even turn to a decrease.

410 Under the combined effects of increased temperature and variations in precipitation,
411 the water yield showed a decrement of 16.5–20.1% during the near future period
412 (Figure 7). At the end of this century, due to the increase of precipitation, the water
413 yield would be no longer continuously reduced, and the decline rate was similar to that
414 the near future period (15–19.5%). Table 6 indicated that water yield had a larger range
415 of variation and correlation than AET and soil water. Figure 8 (a) showed that during
416 the base period, the lowest level of water yield occurred in January, and then increased
417 sharply in May. Water yield peaked in July and decreased after September. From Figure
418 8 (d), we found that the water yield in February, March and November showed an
419 obvious increasing trend compared with the historical period. The highest change was
420 in February, with a change rate of 39.1–129%. The relative changes were also obvious
421 because of the small value of absolute water yield in winter. Besides, water yield was
422 projected to decrease from May to August in each scenario. Figure S6 was the change
423 of water yield during two future periods. We found that water yield in most HRUs
424 would decrease under three RCPs, which was related to the obvious increase of AET.
425 The water yield was predicted to increase only in a few areas, mainly distributed in the
426 southeast of the basin, with the variation range of 1–70 mm. Compared with the near
427 future period, the decline of water yield at the end of this century was reduced, which

might be caused by the increase of rainfall.

4 Discussion

4.1 Intense climate change and potential threats

Our study found that the climate in HYRB would become wetter in terms of the changes of precipitation, especially during far future period under the RCP 8.5 scenarios. The rainfall was projected to increase by 7.3–7.8% for the near future period and 9.0–17.9% for the far future period. Increased precipitation will have a positive effect on AET, soil water, and water yield in study area. The result of the increases in precipitation was generally in line with Feng *et al.* (2016) and Li *et al.* (2008). Compared with summer (June, July, and August), the monthly dynamics of precipitation in other months was more obvious, which may affect the monthly variation of hydrological components in HYRB.

For temperature, the results suggested an increase in both maximum and minimum temperature in the future, and this increasing trend of future temperature is consistent with that in the historical period (Figure S1). During the near future period, the raises of temperature were projected to be substantially similar under RCP 2.6, RCP 4.5, and RCP 8.5, indicating that the different emissions scenarios would not lead to significantly different temperature responses. However, the increase in temperature began to diverge under different emission scenarios during the far future, since the temperature increase was generally 3 °C more under RCP 8.5 than under RCP 2.6. Furthermore, Figure 6 showed that projected increment of maximum temperature were slower than that of minimum temperature, which is consistent with most areas around

450 the world and might lead to a decline in diurnal temperature range (DTR) and
451 considerably affect the growth of vegetation (Donat *et al.*, 2013; Feng *et al.*, 2018;
452 Morak *et al.*, 2013). According to the fifth assessment report (AR5) of IPCC, the
453 simulation results showed that the global average temperature rise could reach 2.6–
454 4.8 °C by the end of the 21st century (Stocker *et al.*, 2013), with the temperature
455 projected to increase more at higher elevations and latitudes (Hu *et al.*, 2014; Luo *et al.*,
456 2019). Previous studies have shown that the temperature changes in the Qinghai-
457 Tibetan Plateau region and the polar regions were more severe than that in other areas
458 (Gao *et al.*, 2012; Overland *et al.*, 2014). As it is climatically sensitive and ecologically
459 fragile, the HYRB region and its environment have been significantly affected by
460 climate change. For example, the wetland ecosystem in the HYRB plays an
461 irreplaceable role in water source conservation, run-off adjustment, and biodiversity
462 maintenance. Climate change will make future efforts to restore and manage wetlands
463 more complex (Erwin, 2008). Consequently, the increasing temperature may cause
464 serious disturbances to the ecological structure and degradation of ecosystem functions,
465 posing a threat to the safety of ecosystems in the middle and lower reaches of the Yellow
466 River Basin.
467
468 4.2 Projected hydrologic changes and influencing climate factors
469 Quantifying the influence of climate factors on hydrological processes is essential
470 for water resources management, especially in semi-arid region. The AET was
471 projected to increase by 31.9–35.3% for the near future period and up to 33.5–54.3%

for the far future period, which was relative to the combined influence of precipitation and temperature. While as for monthly change, the increase in AET in May, June, July, and August was less than other periods. This was due to the reason that the change in precipitation in same period was small, although the temperature increment was similar to other periods. Therefore, the change in temperature made the AET in whole area increase, but the monthly scale change of AET would be greatly affected by precipitation. The warm and wet climate could lead to a downward trend in soil water in the future. The raise of rainfall might have a positive effect on soil water, but the increment of AET due to temperature would result in a decreasing trend of it. Also, due to severe temperature rise, soil water was predicted to continue to decline during far future period, which meant that in the study area, temperature dominated changes in soil water.

The water yield would reduce by 16.5~20.1% for the near future period, which may imply that the HYRB would be under a severe water stress during the mid-century period. The magnitude of the decline in water yield obtained from this study was a little higher than that from Lin *et al.* (2012), who reported a decrease of about 9.5% (2020s) under the A2 scenario in the HYRB. We found that the water yield showed a decreasing trend from May to August both in two periods. The decline of water yield was due to the increase in AET caused by warming, even if the precipitation was also raising during the same period. So the increase in ET would be the main cause for water yield decrease. Meng *et al.* (2016) found that runoff in the HYRB decreased by about 20% in the 2000s, during which precipitation contributed for 3% to the runoff reduction, while the

494 increase in AET accounted for 97%. Besides, due to strong warming over the region,
495 AET has been playing an increasingly important role in influencing runoff changes in
496 recent decades. In the end of this century, driven by the increased precipitation, water
497 yield would no longer continue to decrease, with a decline by 15–19.5% for the far
498 future period. Hence the variation of temperature would dominate the changes in water
499 yield in the HYRB, while rainfall can affect it to some extent.
500
501 4.3 Implication
502 The climate warming has been regarded as an undoubted fact and could further exert
503 adverse effects on the soil water yield, which can alert decision makers for the potential
504 risks, including drought. For example, the reduction of water yield in May to August
505 due to the increment of temperature in the HYRB could be an indicator of reduced water
506 availability in the growing season. Therefore, there was a concern about steady water
507 supply for industrial purposes and crop irrigation not only in the HYRB, but also in the
508 whole Yellow River Basin. Besides, the raising AET and the resulting decline of soil
509 water, especially in irrigation period (May to August), would cause an increasing
510 potential of water stress on crop growth and a resulting increase in water demand for
511 irrigation. Therefore, the reduction in water yield in the HYRB and the increase in
512 irrigation demand require watershed managers to pay attention to the more effective
513 water-use schemes and optimizing effective water-saving irrigation equipment.
514 Many semi-arid regions have the characteristics of water shortage, fragile natural
515 resources, obvious climate change, and great social pressure (Krol *et al.*, 2006).

Integrated studies including climatology and hydrology are required to evaluate possible strategies to make semi-arid areas less susceptible to current and changing climate. Our modeling study provided a proper perspective for investigating the main influencing climate factors of the hydrological components in semi-arid area. This is certainly informative and valuable for people who are interested in the modeling research related to water cycles and its response to climate change, and a better understanding of climatic and hydrological changes in semi-arid areas is highly required to formulate specific and suitable strategies in water resources management (Shen *et al.*, 2019). Besides, climate change dominated the hydrological shifts in alpine region (Yang *et al.*, 2019). Considering the co-effects of both climate and land cover changes on the hydrological cycle, such a headwater area with minimal disturbance by human activities is suitable for diagnosing the historical changes without the challenge of disentangling the land cover changes. In general, although this research is a case study, out results can not only be helpful for understanding the hydrological responses to climate change in semi-arid areas and alpine areas, but also demonstrates the necessity to predict future climate and water cycle changes at local areas, especially when seeking decision support, which can help managers to develop adaptive strategies to mitigate risks and benefit the public.

4.4 Limitations and uncertainties

The soil type, land use, and anthropogenic activities have a great influence on hydrological components, and this may lead to over/under-estimation of the

hydrological components. Besides, previous studies have indicated that high-altitude catchments would experience more complex hydrological changes because of the important role of glaciers, snowmelt, and freeze-thaw process of soil in the water balance (Wang *et al.*, 2015), while we did not take these processes into account in this study because of the model simulation ability. In the future, we will carry out relevant researches. Furthermore, there are inherent uncertainties in the GCMs processes (Zhou *et al.*, 2015). Although out study adopted the arithmetic ensemble averages from the hydrological model outputs that are driven by the eight GCMs to address this uncertainty, due to the complexities involved in the climate change phenomenon, accurately predicting future climate change is very difficult (Knutti and Sedláček, 2012).

5 Conclusions

In this study, we investigated the projection of future climate and its impacts on key hydrological components in the HYRB. The SWAT was calibrated and evaluated for the HYRB. The model performed successfully with satisfactory NSE, R^2, and PBIAS values. Temporally, AET showed an significantly increasing trend during 1976–2015, while soil water and water yield decreased slightly. Spatially, these key hydrological components exhibited a substantial heterogeneity. The precipitation projections indicated that there would be a slight increase of 7.3–7.8% during the near future period and an increase by 9.0–17.9% during the far future period. The climate projections showed a warming of 1.3–1.9 °C for the near future period and 1.5–4.5 °C for the far future period for the maximum temperature. The corresponding values for the minimum

560 temperature were 1.2–1.8 °C and 1.3–4.5 °C. And the projected changes in the
561 maximum temperature were slower than those in the minimum temperature in January,
562 February, March, November, and December. Due to the wetter and warmer climate,
563 AET was predicted to increase dramatically under three RCPs, and there would be an
564 increment in the whole basin compared with historical period. As for soil water, there
565 would be a slight decline of 3.1–6.1% during the near future period and a decrease of
566 4.2–13.3% during the far future period. The spatial changes would be much
567 complicated, but soil water in most HRUs would show a decreasing trend mainly
568 caused by warming. The synergistic effect of the climate change would result in a 16.5–
569 20.1% reduction in water yield during the near future period. In the end of this century,
570 driven by the increased precipitation, water yield would no longer continue to decrease,
571 with a decline by 15–19.5%. So in the HYRB, the variation of temperature would
572 dominate the changes in water yield in the HYRB, while rainfall can affect it to some
573 extent. Besides, the obvious reduction of water yield from May to August would lead
574 to more severe water crisis not only in study area, but also in the whole Yellow River
575 basin.

576 Our study examined the spatiotemporal hydrological dynamics in the HYRB under
577 future climate change conditions. The prediction facilitates the development and
578 implementation of an effective water management plan in advance to minimize
579 potential negative water resources issues in the Yellow River basin. To achieve even
580 more reliable results, future research should consider other factors besides climate
581 change, such as land use changes and increased CO_2 concentrations due to human

activities. We will address this in our future studies.

6 Acknowledgments

This study was funded by the National Key Research and Development Program of China (2019YFC0507403), the Strategic Priority Research Program of Chinese Academy of Sciences (XDB40020205), the National Science Foundation of China (31961143011), and National Thousand Youth Talent Program of China. We also thank the HPCC Platform in Xi'an Jiaotong University for computing equipment and computer maintenance.

Declarations

The authors declare that they have no known competing financial interests or personal relationships that could have appeared to influence the work reported in this paper.

Data Availability Statement

The data that support the findings of this study are available from the corresponding author upon reasonable request.

Appendix 1. Model performance assessment

To measure the model performance, the Nash-Sutcliffe Efficiency (NSE) (Mandeville *et al.*, 1970), the coefficient of determination (R^2) , and the percentage bias

604 (PBIAS) were used in this study. These criteria were calculated as follows:

$$NSE = 1 - \frac{\sum_{i=1}^{n}(Q_{m.i} - Q_{s,i})^2}{\sum_{i=1}^{n}(Q_{m.i} - Q_{m,avg})^2} \quad (1)$$

$$R^2 = \frac{[\sum_{i=1}^{n}(Q_{m.i} - Q_{m,avg})(Q_{s.i} - Q_{s,avg})]^2}{\sum_{i=1}^{n}(Q_{m.i} - Q_{m,avg})^2 \sum_{i=1}^{n}(Q_{s.i} - Q_{s,avg})^2} \quad (2)$$

$$PBIAS = \frac{\sum_{i=1}^{n}(Q_{s.i} - Q_{m,i})}{\sum_{i=1}^{n} Q_{m.i}} \times 100\% \quad (3)$$

605 where $Q_{m.i}$ and $Q_{s,i}$ are measured and simulated streamflow at each time step i;
606 $Q_{m,avg}$ and $Q_{s,avg}$ are the mean measured and simulated streamflow; and n is the
607 number of time steps.

608 The NSE describes the explained variance for the observed values over time that is
609 accounted for by the model (Green and Griensven, 2008). The PBIAS measures the
610 average difference between observation and simulation. The closer NSE and R^2 are to
611 1, and PBIAS to 0, the better the SWAT model performs.

612

613 Appendix 2. Bilinear interpolation downscaling method

614 Bilinear interpolation, as an extension of linear interpolation, is used to interpolate
615 functions of two variables (e.g., x and y) on a rectilinear 2D grid in mathematics
616 (*https://en.wikipedia.org/wiki/Bilinear_interpolation*). The method is described as follows:

617 Suppose get the value of the unknown function f at point $P = (x, y)$. It's assumed
618 that we know the value of the four points of the function f at $Q_{11} = (x_1, y_1)$, $Q_{12} =$
619 (x_1, y_2), $Q_{21} = (x_2, y_1)$, $Q_{22} = (x_2, y_2)$ (Figure S2).

620 First, linear interpolation is performed in the x-direction:

$$f(R_1) \approx \frac{x_2 - x}{x_2 - x_1} f(Q_{11}) + \frac{x - x_1}{x_2 - x_1} f(Q_{21}) \quad (5)$$

where, $R_1 = (x, y_1)$,

$$f(R_2) \approx \frac{x_2 - x}{x_2 - x_1} f(Q_{12}) + \frac{x - x_1}{x_2 - x_1} f(Q_{22}) \tag{6}$$

where, $R_2 = (x, y_2)$.

Then, linear interpolation is performed in the y-direction:

$$f(P) \approx \frac{y_2 - y}{y_2 - y_1} f(R_1) + \frac{y - y_1}{y_2 - y_1} f(R_2) \tag{7}$$

Finally, the desired estimate of $f(x, y)$:

$$\begin{aligned} f(x,y) \approx & \frac{f(Q_{11})}{(x_2 - x_1)(y_2 - y_1)}(x_2 - x)(y_2 - y) \\ & + \frac{f(Q_{21})}{(x_2 - x_1)(y_2 - y_1)}(x - x_1)(y_2 - y) \\ & + \frac{f(Q_{12})}{(x_2 - x_1)(y_2 - y_1)}(x_2 - x)(y - y_1) \\ & + \frac{f(Q_{22})}{(x_2 - x_1)(y_2 - y_1)}(x - x_1)(y - y_1) \end{aligned} \tag{8}$$

References

Abbaspour KC, Yang J, Maximov I, Siber R, Bogner K, Mieleitner J*, et al.*, 2007. Modelling hydrology and water quality in the pre-alpine/alpine Thur watershed using SWAT. *Journal of Hydrology,* **333,** (2), 413-430.

Andrianaki M, Shrestha J, Kobierska F, Nikolaidis NP, Bernasconi SM, 2019. Assessment of SWAT spatial and temporal transferability for a high-altitude glacierized catchment. *Hydrology Earth System Sciences,* **23,** (8), 3219-3232.

Arnold JG, Srinivasan R, Muttiah RS, Williams JR, 1998. Large area hydrologic modeling and assessment part I: model development *Jawra Journal of the American Water Resources Association,* **34,** (1), 73-89.

Bae DH, Koike T, Awan JA, Lee MH, Sohn KH, 2015. Climate change impact assessment on water resources and susceptible zones iIdentification in the Asian monsoon region. *Water Resources Management,* **29,** (14), 5377-5393.

Berg A, Sheffield J, Milly PCD, 2017. Divergent surface and total soil moisture projections under global warming. *Geophysical Research Letters,* **44,** (1), 236-244.

Chen H, Xu C-Y, Guo S, 2012. Comparison and evaluation of multiple GCMs, statistical downscaling and hydrological models in the study of climate change impacts on runoff. *Journal of Hydrology,* **434-435**, 36-45.

Chen L, Liu C, Li Y, Wang G, 2007. Impacts of climatic factors on runoff coefficients in source regions of the Huanghe River. *Chinese Geographical Science,* **17,** (1), 047-055.

Christensen NS, Wood AW, Voisin N, Lettenmaier DP, Palmer RN, 2004. The effects of climate change on the hydrology and water resources of the Colorado River basin. *Climatic Change,* **62,** (1-3),

337-363.
Chu H, Wei J, Li J, Li T, 2018. Investigation of the relationship between runoff and atmospheric oscillations, sea surface temperature, and local-scale climate variables in the Yellow River headwaters region. *Hydrological Processes,* **32,** (10), 1434-1448.
Coles A, McConkey B, McDonnell J, 2017. Climate change impacts on hillslope runoff on the northern Great Plains, 1962–2013. *Journal of Hydrology,* **550**, 538-548.
Cuo L, Zhang Y, Gao Y, Hao Z, Cairang L, 2013. The impacts of climate change and land cover/use transition on the hydrology in the upper Yellow River Basin, China. *Journal of Hydrology,* **502**, 37-52.
Donat M, Alexander L, Yang H, Durre I, Vose R, Dunn R*, et al.*, 2013. Updated analyses of temperature and precipitation extreme indices since the beginning of the twentieth century: The HadEX2 dataset. *Journal of Geophysical Research Atmospheres,* **118,** (5), 2098-2118.
Donnelly C, Greuell W, Andersson J, Gerten D, Pisacane G, Roudier P*, et al.*, 2017. Impacts of climate change on European hydrology at 1.5, 2 and 3 degrees mean global warming above preindustrial level. *Climatic Change,* **143,** (1), 13-26.
Erwin KL, 2008. Wetlands and global climate change: the role of wetland restoration in a changing world. *Wetlands Ecology and Management,* **17,** (1), 71.
Feng R, Yu R, Zheng H, Gan M, 2018. Spatial and temporal variations in extreme temperature in Central Asia. *International Journal of Climatology,* **38**, e388-e400.
Feng T, Yang T, Wang X, Li Z, Yang L, Liu P, 2016. Influence of climate change on hydrologic regime of the Yellow River source region. *Water Resources and Power,* **034,** (007), 11-15.
Flügel WA, 2010. Delineating hydrological response units by geographical information system analyses for regional hydrological modelling using PRMS/MMS in the drainage basin of the River Bröl, Germany. *Hydrological Processes,* **9,** (3-4), 423-436.
Gao G, Fu B, Wang S, Liang W, Jiang X, 2016. Determining the hydrological responses to climate variability and land use/cover change in the Loess Plateau with the Budyko framework. *Science of the Total Environment,* **557-558**, 331-342.
Gao H, He X, Ye B, Pu J, 2012. Modeling the runoff and glacier mass balance in a small watershed on the Central Tibetan Plateau, China, from 1955 to 2008. *Hydrological Processes,* **26,** (11), 1593-1603.
Gassman P, Reyes M, Green C, Arnold J, 2007. The soil and water assessment tool: Historical development, applications, and future research directions. *Transactions of the ASABE,* **50**, 1211-1250.
Giorgi F, Hurrell JW, Marinucci MR, Beniston M, 2010. Elevation dependency of the surface climate change signal: A model study. *Journal of Climate,* **10,** (2), 288-296.
Green CH, Griensven Av, 2008. Autocalibration in hydrologic modeling: Using SWAT2005 in small-scale watersheds. *Environmental Modelling & Software,* **23,** (4), 422-434.
Guo Z, Wang G, Shen Y, Cheng G, 2004. Plant species diversity of grassland plant communities in permafrost regions of the northern Qinghai-Tibet Plateau. *Acta Ecologica Sinica,* **24,** (1), 149-155.
Hartman MD, Baron JS, Lammers RB, Cline DW, Band LE, Liston GE*, et al.*, 1999. Simulations of snow distribution and hydrology in a mountain basin. *Water Resources Research,* **35,** (5), 1587-1603.
Holden PB, Edwards NR, Ridgwell A, Wilkinson RD, Fraedrich K, Lunkeit F*, et al.*, 2018. Climate–carbon cycle uncertainties and the Paris Agreement. *Nature Climate Change,* **8,** (7), 609-613.

Hu Y, Maskey S, Uhlenbrook S, Zhao H, 2011. Streamflow trends and climate linkages in the source region of the Yellow River, China. *Hydrological Processes,* **25,** (22), 3399-3411.

Hu Z, Zhang C, Hu Q, Tian H, 2014. Temperature changes in Central Asia from 1979 to 2011 based on multiple Datasets. *Journal of Climate,* **27,** (3), 1143-1167.

Jian T, Zhang Y, Zhu J, Jiang Y, Yi X, 2014. Elevation-dependent temperature change in the Qinghai–Xizang Plateau grassland during the past decade. *Theoretical & Applied Climatology,* **117,** (1-2), 61-71.

Kendall, MauriceG, 1979. *The advanced theory of statistics.* C. Griffin.

Knutti R, Sedláček J, 2012. Robustness and uncertainties in the new CMIP5 climate model projections. *Nature Climate Change,* **3**, 369.

Krol M, Jaeger A, Bronstert A, Güntner A, 2006. Integrated modelling of climate, water, soil, agricultural and socio-economic processes: A general introduction of the methodology and some exemplary results from the semi-arid north-east of Brazil. *Journal of Hydrology,* **328,** (3-4), 417-431.

Li L, Hao ZC, Wang JH, Wang ZH, Yu ZB, 2008. Impact of future climate change on runoff in the head region of the Yellow River. *Journal of Hydrologic Engineering,* **13,** (5), 347-354.

Lin L, Shen H, Dai S, Xiao J, Shi X, 2012. Response of runoff to climate change and its future tendency in the source region of Yellow River. *Journal of Geographical Sciences,* **22,** (3), 431-440.

Lin P, He Z, Du J, Chen L, Jing L, 2018. Impacts of climate change on reference evapotranspiration in the Qilian Mountains of China: Historical trends and projected changes. *International Journal of Climatology***,** (5), 2980– 2993.

Liu L, Xu H, Wang Y, Jiang T, 2017. Impacts of 1.5 and 2 °C global warming on water availability and extreme hydrological events in Yiluo and Beijiang River catchments in China. *Climatic Change,* **145,** (1), 145-158.

Liu X, Chen B, 2015. Climatic warming in the Tibetan Plateau during recent decades. *International Journal of Climatology,* **20,** (14), 1729-1742.

Lu W, Wang W, Shao Q, Yu Z, Hao Z, Xing W*, et al.*, 2018. Hydrological projections of future climate change over the source region of Yellow River and Yangtze River in the Tibetan Plateau: A comprehensive assessment by coupling RegCM4 and VIC model. *Hydrological Processes,* **32,** (13), 2096-2117.

Lubchenco J, 1998. Entering the century of the environment: A new social contract for science. *Science,* **279,** (5350), 491.

Luo M, Liu T, Meng F, Duan Y, Bao A, Frankl A*, et al.*, 2019. Spatiotemporal characteristics of future changes in precipitation and temperature in Central Asia. *International Journal of Climatology,* **39,** (3), 1571-1588.

Mandeville AN, O'Connell PE, Sutcliffe JV, Nash JE, 1970. River flow forecasting through conceptual models part III - The Ray catchment at Grendon Underwood. *Journal of Hydrology,* **11,** (2), 109-128.

Meaurio M, Zabaleta A, Boithias L, Epelde AM, Sauvage S, Sánchez-Pérez J-M*, et al.*, 2017. Assessing the hydrological response from an ensemble of CMIP5 climate projections in the transition zone of the Atlantic region (Bay of Biscay). *Journal of Hydrology,* **548**, 46-62.

Meng F, Su F, Yang D, Tong K, Hao Z, 2016. Impacts of recent climate change on the hydrology in the source region of the Yellow River basin. *Journal of Hydrology: Regional Studies,* **6**, 66-81.

Morak S, Hegerl GC, Christidis N, 2013. Detectable Changes in the Frequency of Temperature Extremes. *Journal of Climate,* **26,** (5), 1561-1574.

737 Neupane RP, Ficklin DL, Knouft JH, Ehsani N, Cibin R, 2019. Hydrologic responses to projected climate
738 change in ecologically diverse watersheds of the Gulf Coast, United States. *International*
739 *Journal of Climatology,* **39,** (4), 2227-2243.
740 Oki T, Kanae S, 2006. Global hydrological cycles and world water resources. *Science,* **313,** (5790), 1068-
741 1072.
742 Overland JE, Wang M, Walsh JE, Stroeve JC, 2014. Future Arctic climate changes: Adaptation and
743 mitigation time scales. *Earth's Future,* **2,** (2), 68-74.
744 Patel DP, Srivastava PK, 2013. Flood hazards mitigation analysis using remote sensing and GIS:
745 Correspondence with town planning scheme. *Water Resources Management,* **27,** (7), 2353-2368.
746 Patel PM, Saha D, Shah T, 2020. Sustainability of groundwater through community-driven distributed
747 recharge: An analysis of arguments for water scarce regions of semi-arid India. *Journal of*
748 *Hydrology: Regional Studies,* **29**, 100680.
749 Pereira DdR, Martinez MA, Pruski FF, da Silva DD, 2016. Hydrological simulation in a basin of typical
750 tropical climate and soil using the SWAT model part I: Calibration and validation tests. *Journal*
751 *of Hydrology: Regional Studies,* **7**, 14-37.
752 Piao S, Ciais P, Huang Y, Shen Z, Peng S, Li J*, et al.*, 2010. The impacts of climate change on water
753 resources and agriculture in China. *Nature,* **467,** (7311), 43-51.
754 Shen Y, Guo Y, Zhang Y, Pei H, Brenning A, 2019. Review of historical and projected future climatic
755 and hydrological changes in mountainous semiarid Xinjiang (northwestern China), central Asia.
756 *CATENA,* **187**, 104343.
757 Stocker T, Qin D, Plattner G-K, Tignor M, Allen SK, Boschung J*, et al.*, 2013. Climate Change 2013:
758 The Physical Science Basis. Contribution of Working Group I to the Fifth Assessment Report
759 of the Intergovernmental Panel on Climate Change. *Cambridge University Press Cambridge,*
760 *United Kingdom and New York, NY, USA (2013)*.
761 Sun P, Wu Y, Yang Z, Sivakumar B, Qiu L, Liu S*, et al.*, 2019. Can the Grain-for-Green program really
762 ensure a low sediment load on the Chinese Loess Plateau? *Engineering,* **5,** (5), 855-864.
763 Sun Z, Jia S, Aifeng LV, Zhu W, Gao Y, 2016. Precision estimation of the average daily precipitation
764 simulated by IPCC AR5 GCMs in China. *Journal of Geo-Information Science,* **18(2)**, 227-237.
765 Trenberth KE, Dai A, van der Schrier G, Jones PD, Barichivich J, Briffa KR*, et al.*, 2014. Global warming
766 and changes in drought. *Nature Climate Change,* **4,** (1), 17-22.
767 Wang G, Wang Y, Li Y, Cheng H, 2007. Influences of alpine ecosystem responses to climatic change on
768 soil properties on the Qinghai–Tibet Plateau, China. *CATENA,* **70,** (3), 506-514.
769 Wang R, Yao Z, Liu Z, Wu S, Jiang L, Wang L, 2015. Snow cover variability and snowmelt in a high-
770 altitude ungauged catchment. *Hydrological Processes,* **29,** (17), 3665-3676.
771 Wilby RL, Dawson CW, Barrow EM, 2002. SDSM — a decision support tool for the assessment of
772 regional climate change impacts. *Environmental Modelling & Software,* **17,** (2), 145-157.
773 Wu Y, Liu S, Yan W, Xia J, Xiang W, Wang K*, et al.*, 2016. Climate change and consequences on the
774 water cycle in the humid Xiangjiang River Basin, China. *Stochastic environmental research risk*
775 *assessment,* **30,** (1), 225-235.
776 Xu Z, Zhao F, Li J, 2009. Response of streamflow to climate change in the headwater catchment of the
777 Yellow River basin. *Quaternary International,* **208,** (1), 62-75.
778 Yang J, Reichert P, Abbaspour KC, Xia J, Yang H, 2008. Comparing uncertainty analysis techniques for
779 a SWAT application to the Chaohe Basin in China. *Journal of Hydrology,* **358,** (1), 1-23.
780 Yang K, Wu H, Qin J, Lin C, Tang W, Chen Y, 2014. Recent climate changes over the Tibetan Plateau

781 and their impacts on energy and water cycle: A review. *Global and Planetary Change,* **112**, 79-
782 91.
783 Yang L, Feng Q, Yin Z, Deo RC, Liu W, 2019. Regional hydrology heterogeneity and the response to
784 climate and land surface changes in arid alpine basin, northwest China. *CATENA,* **187**, 104345.
785 Yang L, Feng Q, Yin Z, Wen X, Si J, Li C*, et al.*, 2017. Identifying separate impacts of climate and land
786 use/cover change on hydrological processes in upper stream of Heihe River, Northwest China.
787 *Hydrological Processes,* **31,** (5), 1100-1112.
788 Zhang L, Karthikeyan R, Bai Z, Srinivasan R, 2017. Analysis of streamflow responses to climate
789 variability and land use change in the Loess Plateau region of China. *CATENA,* **154**, 1-11.
790 Zhang L, Nan Z, Yu W, Zhao Y, Xu Y, 2018. Comparison of baseline period choices for separating climate
791 and land use/land cover change impacts on watershed hydrology using distributed hydrological
792 models. *Science of the Total Environment,* **622-623**, 1016-1028.
793 Zhang S, Jia S, Liu C, Cao W, Hao F, Liu J*, et al.*, 2004. Study on the changes of water cycle and its
794 impacts in the source region of the Yellow River. *Science in China Series E: Technological*
795 *Sciences,* **47,** (1), 142-151.
796 Zhang Y, You Q, Chen C, Ge J, 2016. Impacts of climate change on streamflows under RCP scenarios:
797 A case study in Xin River Basin, China. *Atmospheric Research,* **178-179**, 521-534.
798 Zhang Y, Zhang S, Xia J, Hua D, 2013. Temporal and spatial variation of the main water balance
799 components in the three rivers source region, China from 1960 to 2000. *Environmental earth*
800 *sciences,* **68,** (4), 973-983.
801 Zhao F, Wu Y, Qiu L, Bellie S, Bellie S, Zhang F*, et al.*, 2018. Spatiotemporal features of the hydro-
802 biogeochemical cycles in a typical loess gully watershed. *Ecological Indicators,* **91**, 542-554.
803 Zhou G, Wei X, Wu Y, Liu S, Huang Y, Yan J*, et al.*, 2011. Quantifying the hydrological responses to
804 climate change in an intact forested small watershed in Southern China. *Global change biology,*
805 **17,** (12), 3736-3746.
806 Zhou H, Zhao X, Tang Y, Gu S, Zhou L, 2005. Alpine grassland degradation and its control in the source
807 region of the Yangtze and Yellow Rivers, China. *Grassland Science,* **51,** (3), 191-203.
808 Zhou J, He D, Xie Y, Liu Y, Yang Y, Sheng H*, et al.*, 2015. Integrated SWAT model and statistical
809 downscaling for estimating streamflow response to climate change in the Lake Dianchi
810 watershed, China. *Stochastic Environmental Research & Risk Assessment,* **29,** (4), 1193-1210.

811

812

Table captions

Table 1. Information of the eight General Circulation Models (GCMs) used in this study.

Table 2. Calibrated parameter values for the headwater area of the Yellow River Basin.

Table 3. Evaluation of model performance in monthly streamflow simulation at the Tangnaihai gaging station during the twenty-year (1981–2000) calibration and twenty-year (1971–1980, 2001–2010) validation periods.

Table 4.Area percentage of the changing trends of the three key hydrological components during 1976–2015.

Table 5. Variations in annual precipitation, maximum air temperature (TMAX), and minimum air temperature (TMIN) during the near future (NF, 2020–2059) and far future (FF, 2060–2099) periods under RCP 2.6, RCP 4.5, and RCP 8.5 compared with the baseline period (1976–2015). CV denotes the coefficient of variation of model annual averages.

Table 6. Variations in annual AET, soil water, and water yield during the near future (NF, 2020–2059) and far future (FF, 2060–2099) periods under RCP 2.6, RCP 4.5, and RCP 8.5 compared with the baseline period (1976–2015). CV denotes the coefficient of variation of model annual averages.

831 **Figure captions**

832 Figure 1. The location and brief description of the headwater area of the Yellow River
833 Basin, China.

834 Figure 2. Monthly streamflow simulation at the Tangnaihai gaging station during the
835 calibration period (1981–2000) and the validation periods (1971–1980, 2001–
836 2010).

837 Figure 3. Temporal changes in annual AET (actual evapotranspiration), water yield, and
838 soil water during 1976–2015. SD means standard deviation.

839 Figure 4. Spatial distributions of (a-c) annual mean key hydrological components, (d-f)
840 annual trends of key hydrological components, and (g-i) probability density
841 distribution of trends in the HYRB during 1976–2015 on the Hydrologic
842 Response Unit (HRU) level. "///" indicates that the trend has passed the
843 significance test (p<0.05).

844 Figure 5. Ensemble values of annual mean precipitation, maximum and minimum air
845 temperature under three RCPs during the future period of 2020–2099. The
846 blue, green, and red lines represent the historical period, near future (NF,
847 2020–2059), and the far future (FF, 2060–2099) periods, respectively. The
848 shading area denotes the ±1 standard deviation range of model annual
849 averages.

850 Figure 6. (a) Monthly mean precipitation, maximum and minimum air temperature
851 during baseline period (1976–2015). (b) Projected changes in ensemble
852 monthly mean precipitation, (c) maximum and (d) minimum air temperature
853 during the near future (NF, 2020–2059) and far future (FF, 2060–2099)
854 periods under RCP 2.6, 4.5, and 8.5 relative to baseline.

855 Figure 7. Ensemble values of annual mean AET (actual evapotranspiration), soil water,
856 and water yield under three RCPs during the future period of 2020–2099. The
857 green and red lines represent the near future (NF, 2020–2059) and the far

858 future (FF, 2060–2099) periods, respectively. The shading area denotes the
859 ±1 standard deviation range of model annual averages.

860 Figure 8. (a) Monthly AET (actual evapotranspiration), soil water and water yield
861 during the baseline period (1976–2015) and the projected monthly changes in
862 (b) AET, (c) soil water, and (d) water yield during the near future (NF, 2020–
863 2059) and the far future (FF, 2060–2099) periods under the RCP 2.6, 4.5, and
864 8.5 relative to baseline in the HYRB.

865 Figure S1. Temporal changes in annual precipitation, maximum temperature, minimum
866 temperature, wind speed, relative humidity, and solar radiation in the
867 headwater area of the Yellow River Basin (HYRB) during 1966–2015.

868 Figure S2. Bilinear-interpolation schematic diagram.

869 Figure S3. Comparison of observed and GCM-derived (a) monthly precipitation, (b)
870 maximum and (c) minimum temperature in the HYRB during 1986 and 2005.

871 Figure S4. The difference of AET (actual evapotranspiration) between near future
872 (2020–2059) and historical period, far future (2060-2099) and historical
873 period under the RCP 2.6, 4.5, and 8.5.

874 Figure S5. The difference of soil water between near future (2020–2059) and historical
875 period, far future (2060–2099) and historical period under the RCP 2.6, 4.5,
876 and 8.5.

877 Figure S6. The difference of water yield between near future (2020–2059) and historical
878 period, far future (2060–2099) and historical period under the RCP 2.6, 4.5,
879 and 8.5.

880

881 **Table**

882 Table 1. Information of the eight General Circulation Models (GCMs) used in this
883 study.

Model	Institution	Resolution (Lon × Lat)	Time Period
CanESM2	CCCMA, Canada	2.8°× 2.8°	2006-2100
CNRM-CM5	CNRM-CERFACS, France	1.4°×1.4°	2006-2100
GFDL-CM3	GFDL, America	2.0°× 2.5°	2006-2100
GFDL-ESM2G	GFDL, America	2.0°× 2.5°	2006-2100
MIROC-ESM	AORI-NIES-JAMSTEC, Japan	2.8°× 2.8°	2006-2100
MPI-ESM-LR	MPI-M, Germany	1.9°× 1.9°	2006-2100
MRI-CGCM3	MRI, Japan	0.6°× 0.6°	2006-2100
NorESM1-M	NCC, Norway	1.9°×2.5°	2006-2100

884
885

886 Table 2. Calibrated parameter values for the headwater area of the Yellow River Basin.
887

Parameter	Description	Range	Calibrated value/change
CN2	SCS curve number for moisture condition Ⅱ	-10% – 10%	9.7%
ALPHA_BF	Baseflow alpha factor (day)	0.03 – 0.09	0.043
GW_DELAY	Groundwater delay (day)	2.0 – 6.0	4.717
GW_REVAP	Groundwater revap coefficient	0.01 – 0.02	0.018
ESCO	Soil evaporation compensation factor	0.5 – 0.99	0.987
SOL_K	Saturated hydraulic conductivity (mm/h)	-5% – 20%	1.40%
SOL_AWC	Available water capacity of soil layer (mm)	-13% – 10%	9.6%
CH_K2	Main channel conductivity (mm/h)	4.0 – 10.0	9.057
SMTMP	Snowmelt temperature (℃)	-0.5 – 1.28	0.646
SFTMP	Snowfall temperature (℃)	1.51 – 3.13	1.967
TLAPS	Temperature lapse rate	-7.43 – -6.11	-6.37
SOL_Z	Depth from soil surface to the bottom of the layer (mm)	-10% – 5%	-6.1%

888
889

890 Table 3. Evaluation of model performance in monthly streamflow simulation at the
891 Tangnaihai gaging station during the twenty-year (1981–2000) calibration and twenty-
892 year (1971–1980, 2001–2010) validation periods.
893

Period	Average runoff (m^3/s)		R^2	NSE	PBIAS (%)
	Observed	Simulated			
Calibration (1981–2000)	652.72	650.99	0.86	0.85	-0.3
Validation I (1971–1980)	658.34	656.39	0.88	0.87	-0.3
Validation II (2001–2010)	564.14	627.4	0.89	0.82	11.3

894
895

Table 4. Area percentage of the changing trends of the three key hydrological components during 1976–2015.

	Percent area of significant decrease (%)	Percent area of insignificant decrease (%)	Percent area of insignificant increase (%)	Percent area of significant increase (%)
AET	3.95	11.85	10.2	74
Soil water	25.6	25.1	34.3	15
Water yield	0	48.2	51.8	0

Table 5. Variations in annual precipitation, maximum air temperature (TMAX), and minimum air temperature (TMIN) during the near future (NF, 2020–2059) and far future (FF, 2060–2099) periods under RCP 2.6, RCP 4.5, and RCP 8.5 compared with the baseline period (1976–2015). CV denotes the coefficient of variation of model annual averages.

Scenario	RCP 2.6		RCP 4.5		RCP 8.5	
Period	NF	FF	NF	FF	NF	FF
Precipitation change (%)	7.3	9.0	7.6	12.9	7.8	17.9
CV (Precipitation %)	6.2	7.4	6.4	8.9	5.9	11.1
TMAX change (℃)	1.3	1.5	1.6	2.6	1.9	4.5
CV (TMAX %)	8.4	10.5	7.8	10.7	8.1	9.7
TMIN change (℃)	1.2	1.3	1.5	2.4	1.8	4.5
CV (TMIN %)	13.9	17.3	14.6	26.9	17.8	229.2

908 Table 6. Variations in annual AET, soil water, and water yield during the near future
909 (NF, 2020–2059) and far future (FF, 2060–2099) periods under RCP 2.6, RCP 4.5, and
910 RCP 8.5 compared with the baseline period (1976–2015). CV denotes the coefficient
911 of variation of model annual averages.
912

Scenario	RCP 2.6		RCP 4.5		RCP 8.5	
Period	NF	FF	NF	FF	NF	FF
AET change (%)	32	33.5	33.3	41.8	35.3	54.3
CV (AET %)	6.7	8.5	6.6	8.8	6.5	9.6
Soil water change (%)	-3.1	-4.2	-6.1	-9	-6.1	-13.3
CV (Soil water %)	5.6	5.8	3.2	4.2	3.3	5.3
Water yield change (%)	-16.5	-15	-17.8	-16	-20.1	-19.5
CV (Water yield %)	12.3	11.3	13.2	16.3	12	21.8

913
914

915 **Figure**

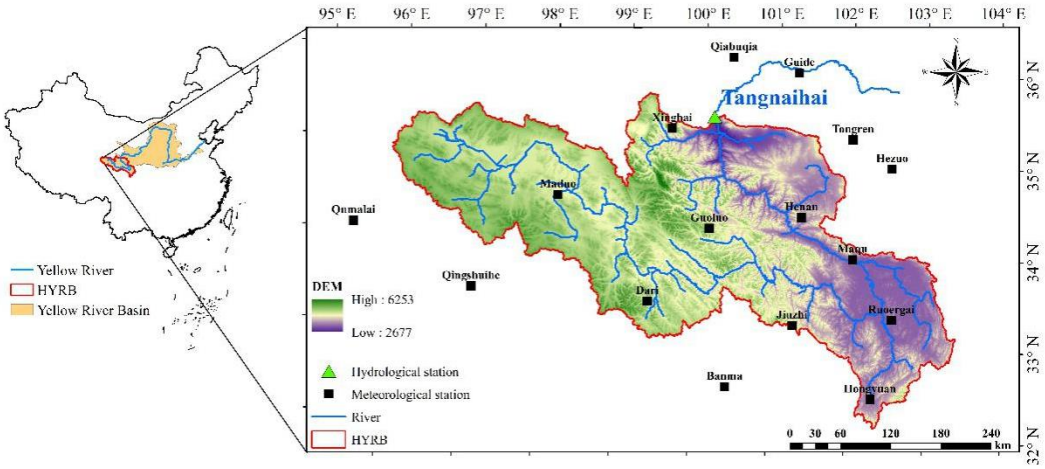

916

917 Figure 1. The location and brief description of the headwater area of the Yellow
918 River Basin (HYRB), China.

919

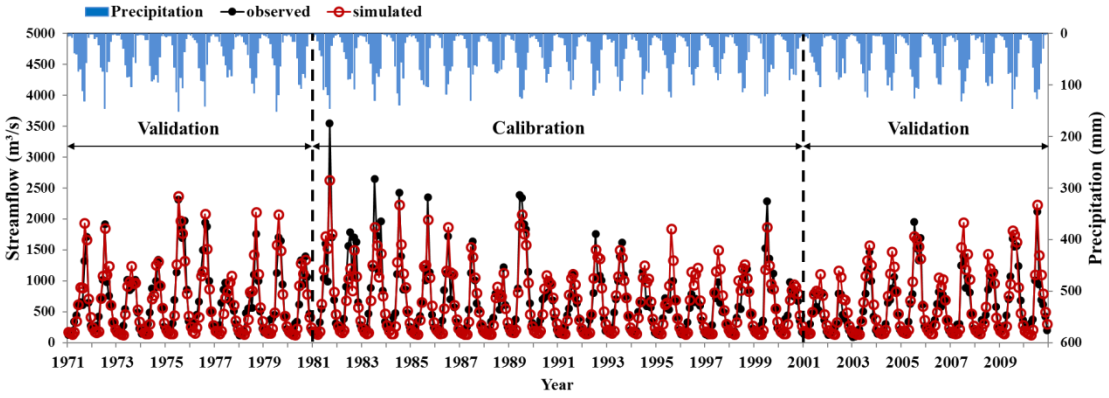

Figure 2. Monthly streamflow simulation at the Tangnaihai gaging station during the calibration period (1981–2000) and the validation periods (1971–1980, 2001–2010).

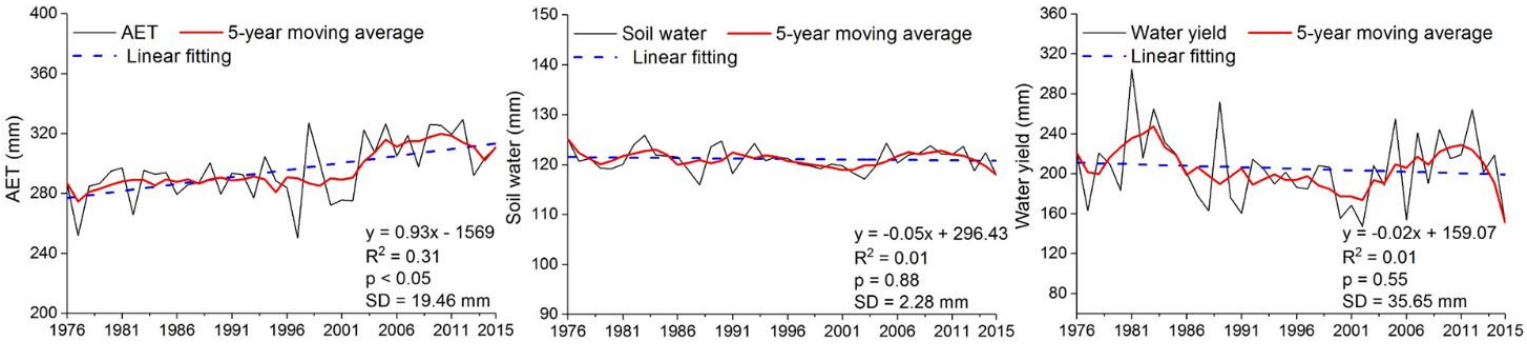

924

925 Figure 3. Temporal changes in annual AET (actual evapotranspiration), water yield,
926 and soil water during 1976–2015. SD means standard deviation.

927

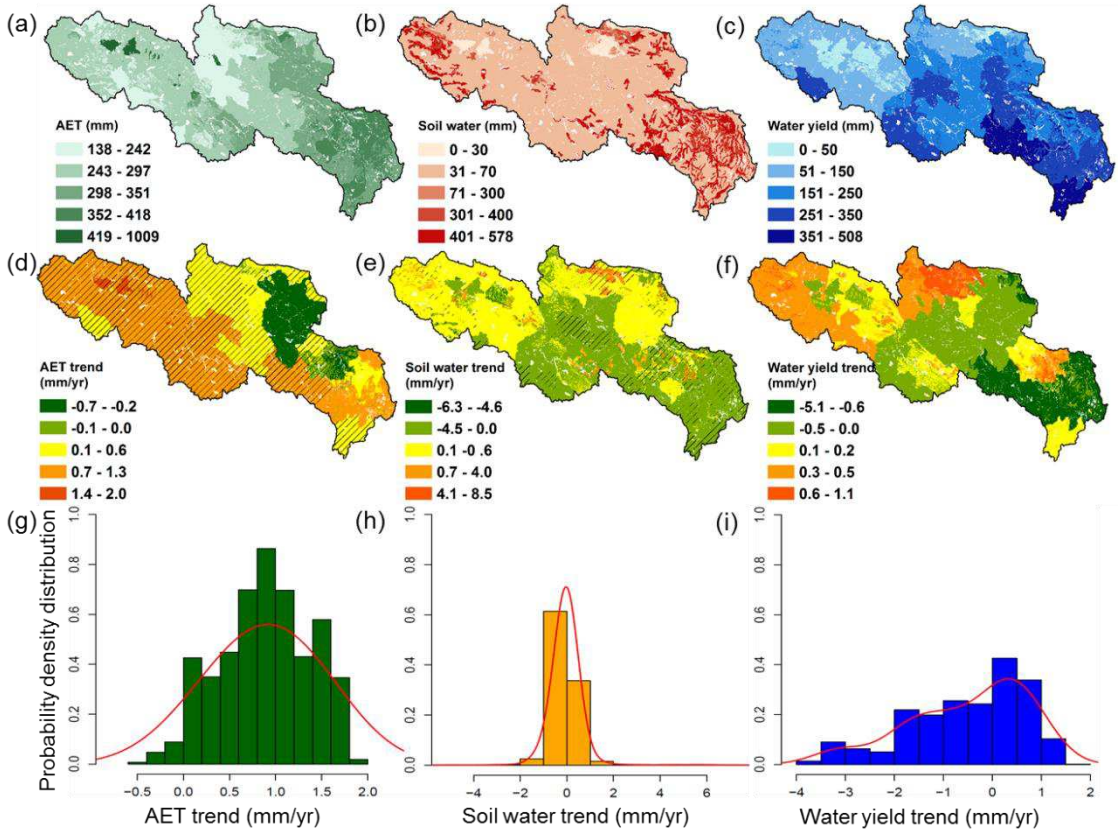

Figure 4. Spatial distributions of (a-c) annual mean key hydrological components, (d-f) annual trends of key hydrological components, and (g-i) probability density distribution of trends in the HYRB during 1976–2015 on the Hydrologic Response Unit (HRU) level. "///" indicates that the trend has passed the significance test (p<0.05).

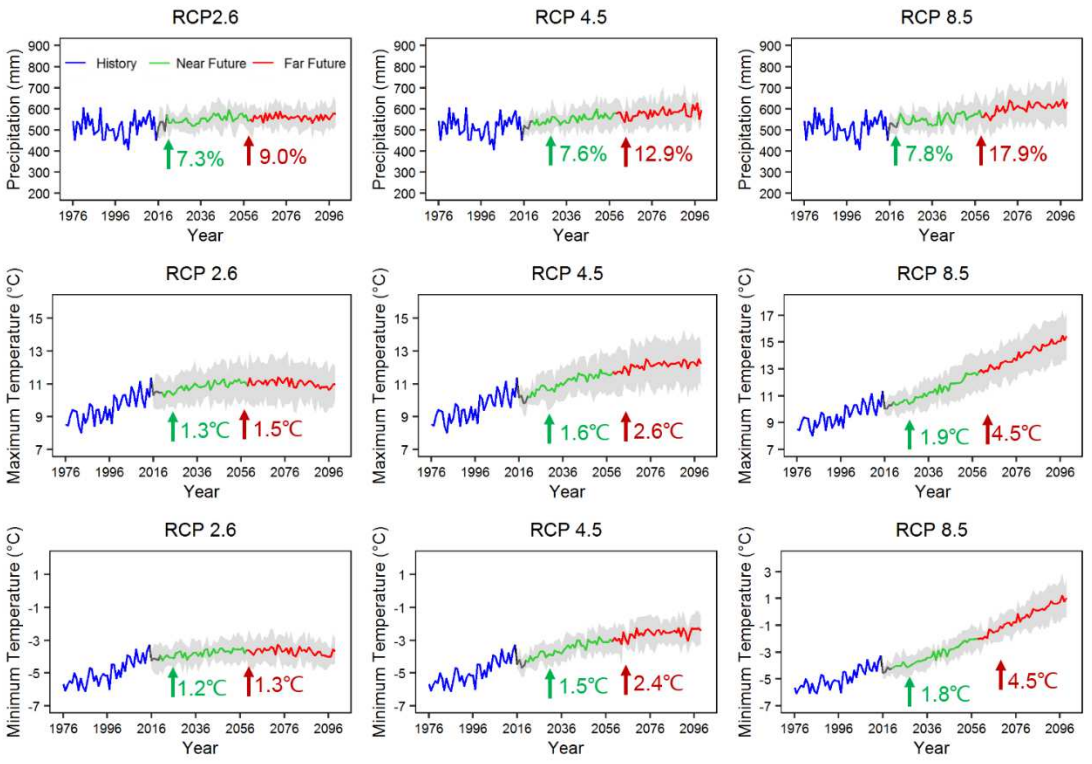

Figure 5. Ensemble values of annual mean precipitation, maximum and minimum air temperature under three RCPs during the future period of 2020–2099. The blue, green, and red lines represent the historical period, near future (NF, 2020–2059), and the far future (FF, 2060–2099) periods, respectively. The shading area denotes the ±1 standard deviation range of model annual averages.

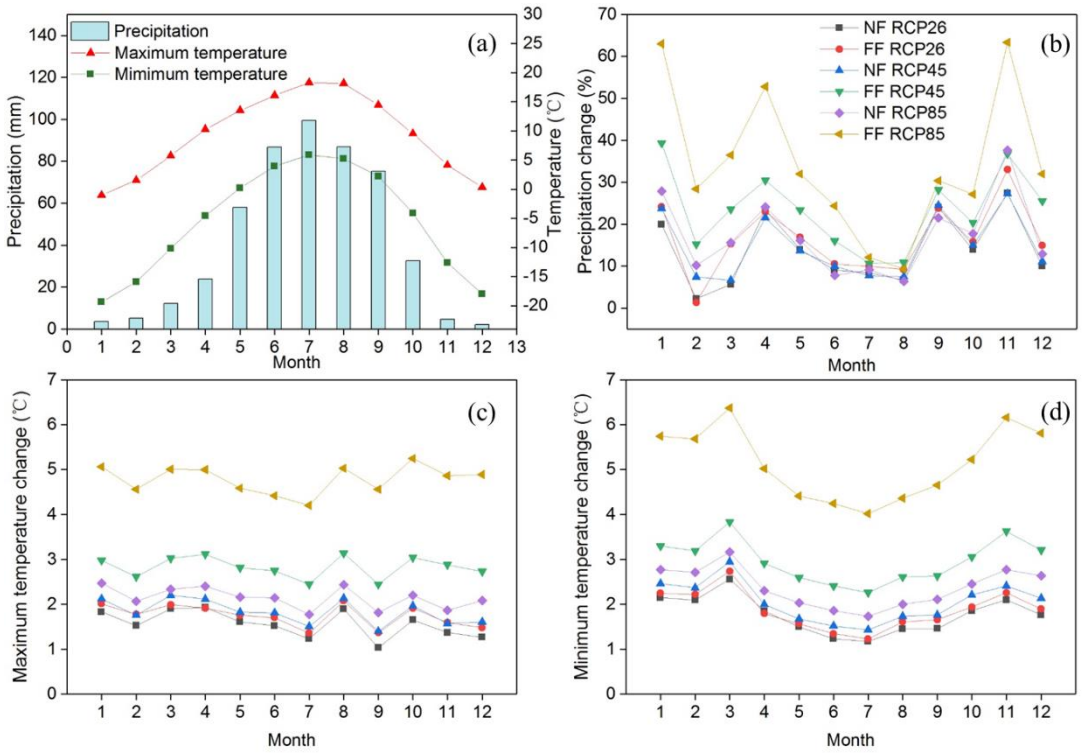

Figure 6. (a) Monthly mean precipitation, maximum and minimum air temperature during baseline period (1976–2015). (b) Projected changes in ensemble monthly mean precipitation, (c) maximum and (d) minimum air temperature during the near future (NF, 2020–2059) and far future (FF, 2060–2099) periods under RCP 2.6, 4.5, and 8.5 relative to baseline.

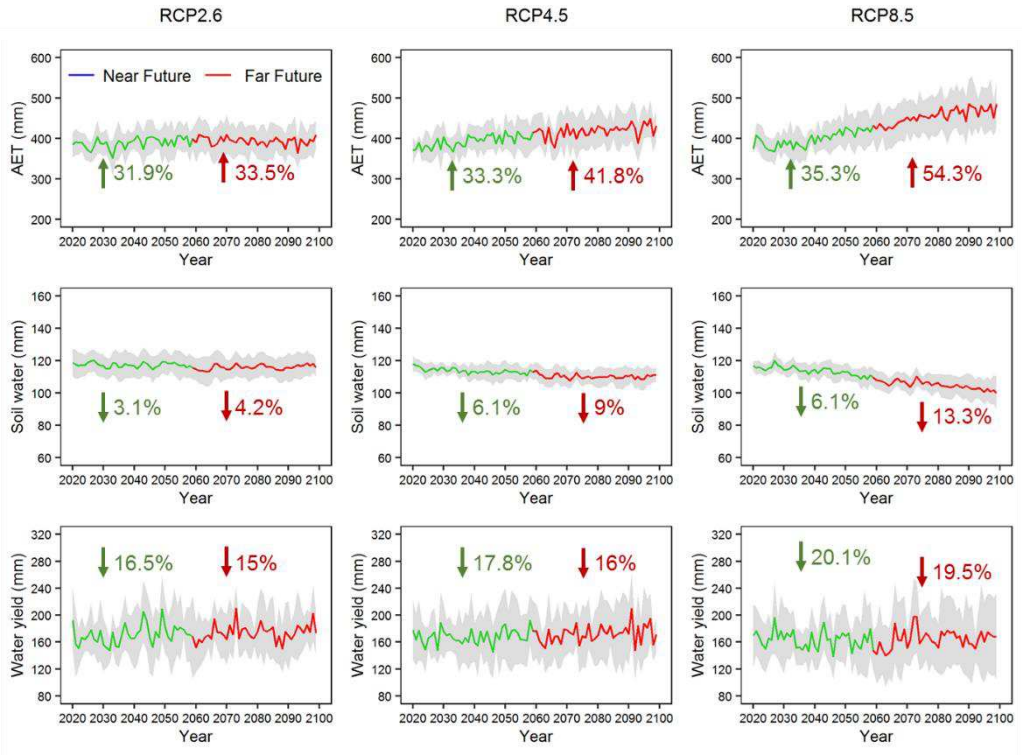

Figure 7. Ensemble values of annual mean AET (actual evapotranspiration), soil water, and water yield under three RCPs during the future period of 2020–2099. The green and red lines represent the near future (NF, 2020–2059) and the far future (FF, 2060–2099) periods, respectively. The shading area denotes the ±1 standard deviation range of model annual averages.

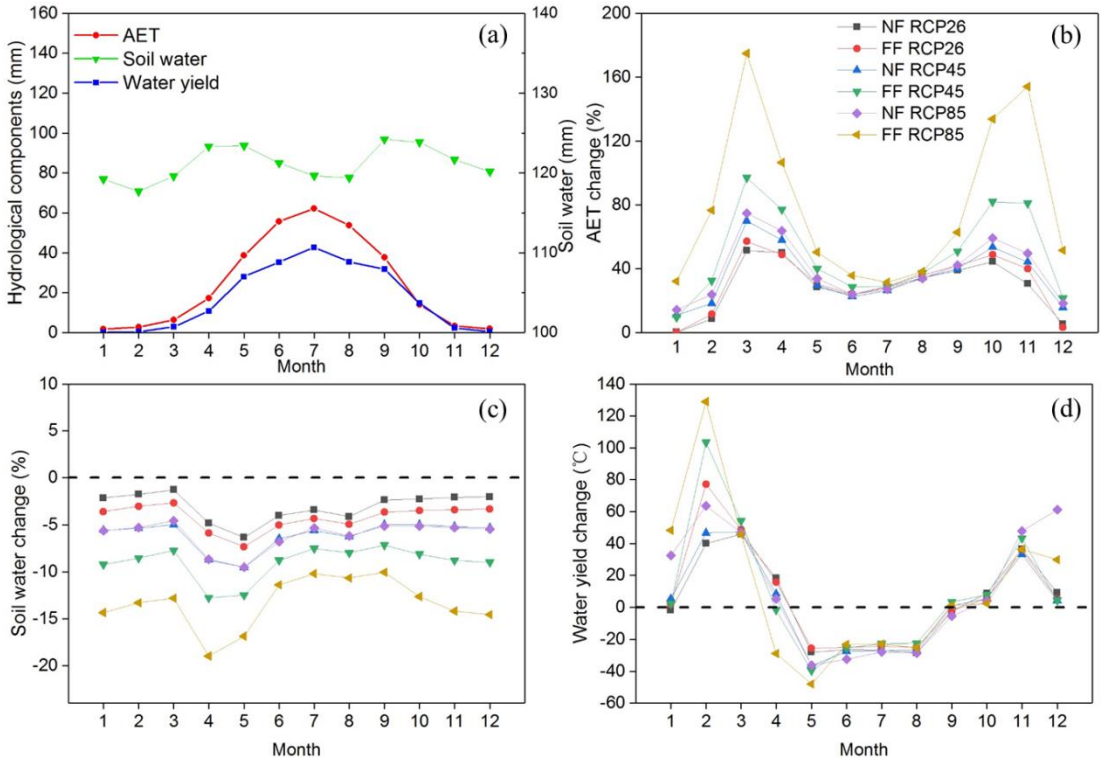

Figure 8. (a) Monthly AET (actual evapotranspiration), soil water and water yield during the baseline period (1976–2015) and the projected monthly changes in (b) AET, (c) soil water, and (d) water yield during the near future (NF, 2020–2059) and the far future (FF, 2060–2099) periods under the RCP 2.6, 4.5, and 8.5 relative to baseline in the HYRB.

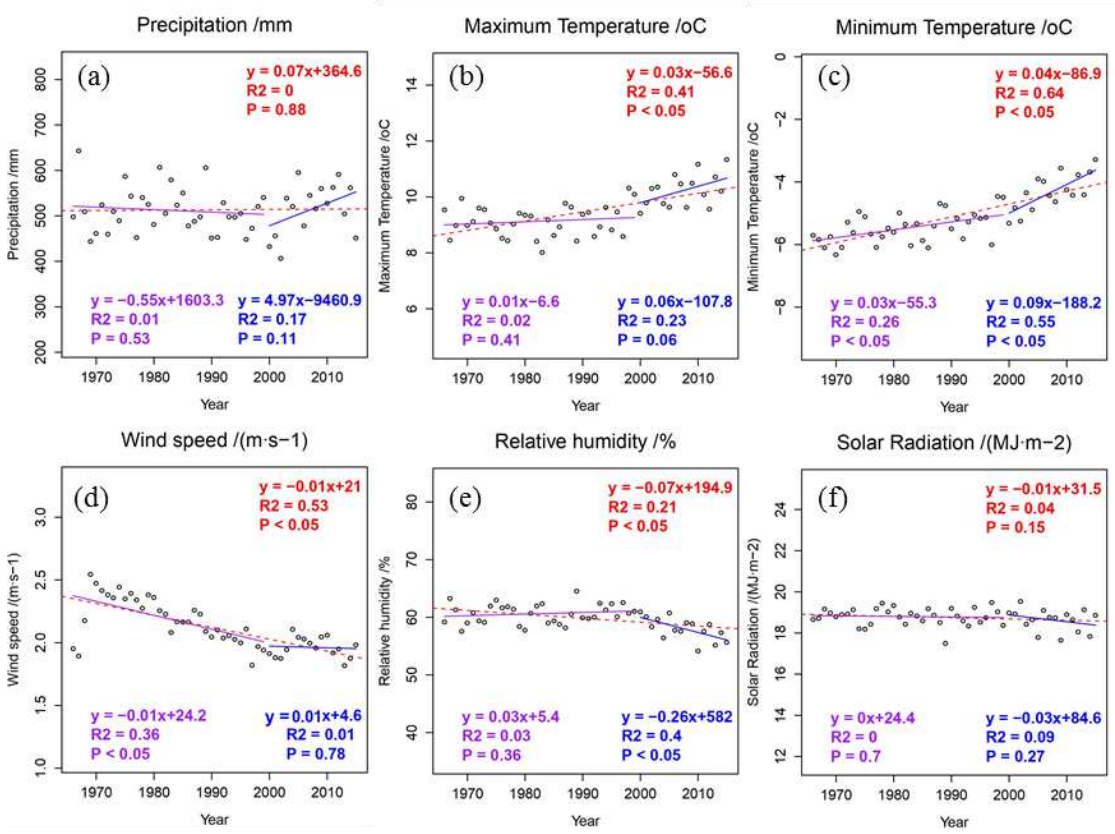

Figure S1. Temporal changes in annual precipitation, maximum temperature, minimum temperature, wind speed, relative humidity, and solar radiation in the headwater area of the Yellow River Basin (HYRB) during 1966–2015.

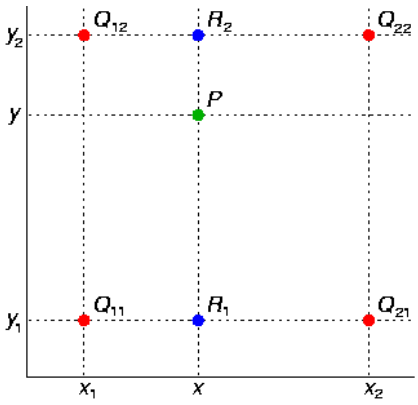

Figure S2. Bilinear-interpolation schematic diagram.

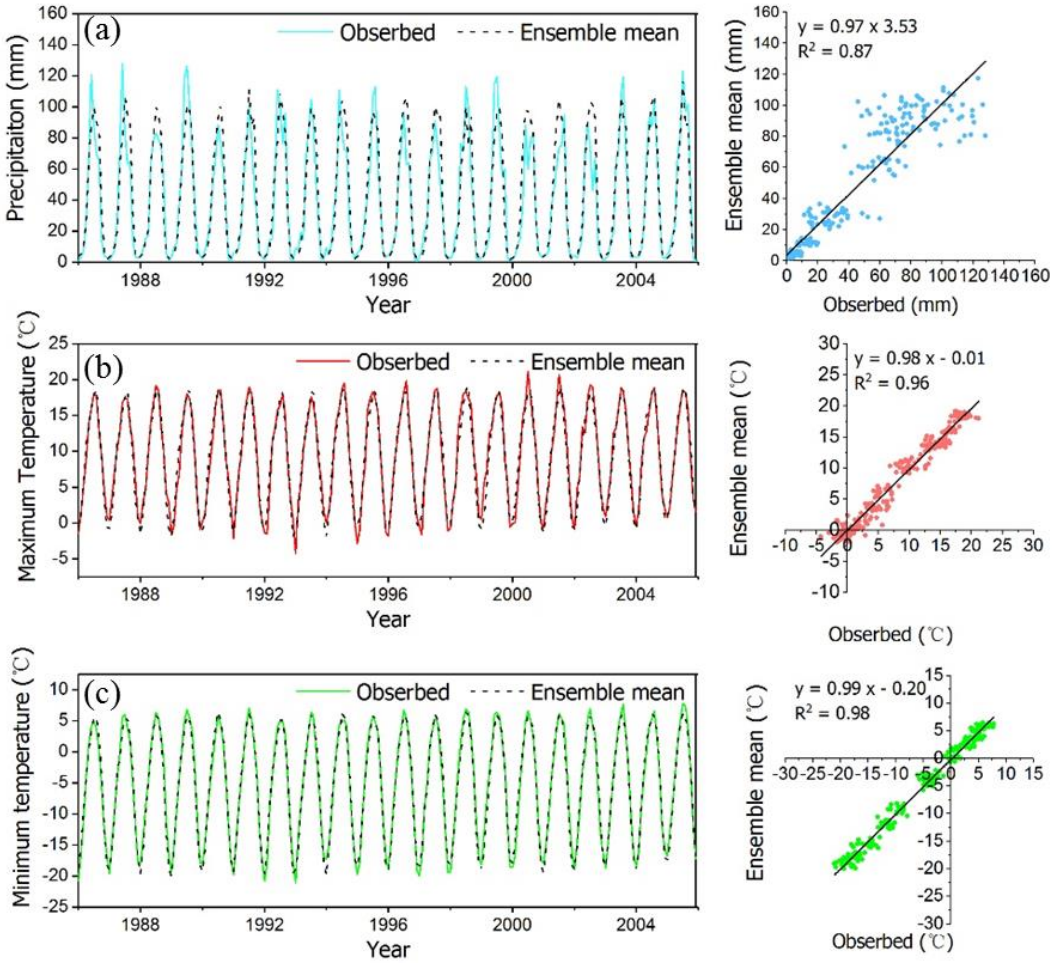

Figure S3. Comparison of observed and GCM-derived (a) monthly precipitation, (b) maximum and (c) minimum temperature in the HYRB during 1986 and 2015.

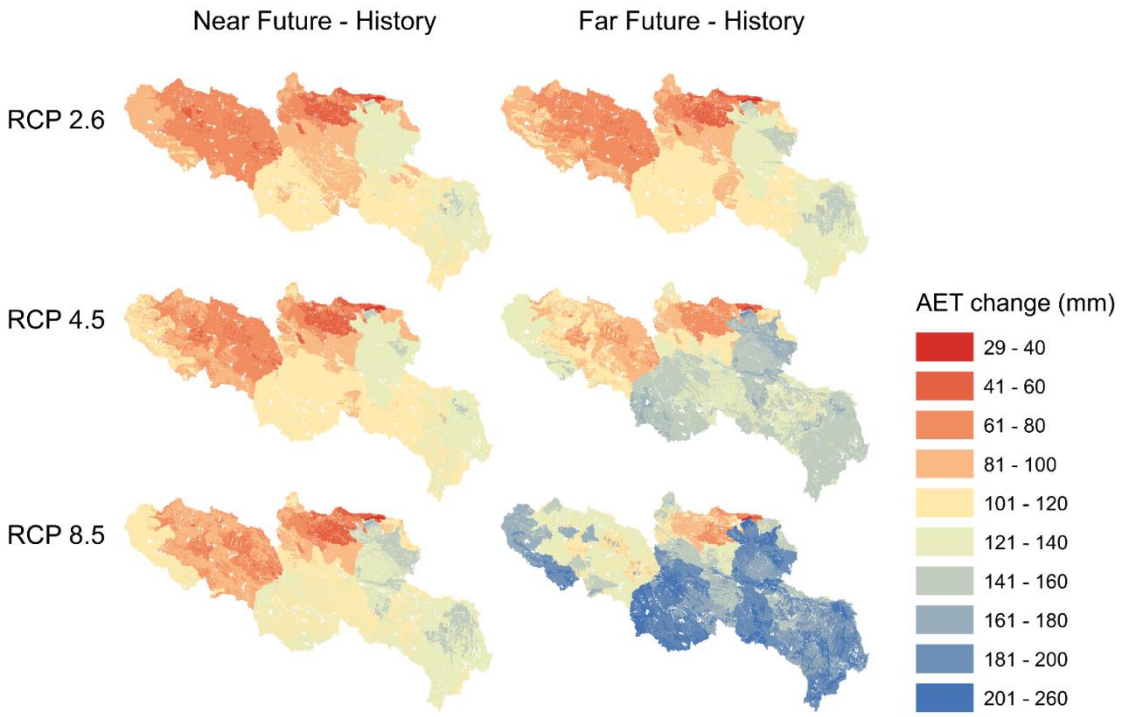

Figure S4. The difference of AET (actual evapotranspiration) between near future (2020–2059) and historical period, far future (2060-2099) and historical period under the RCP 2.6, 4.5, and 8.5.

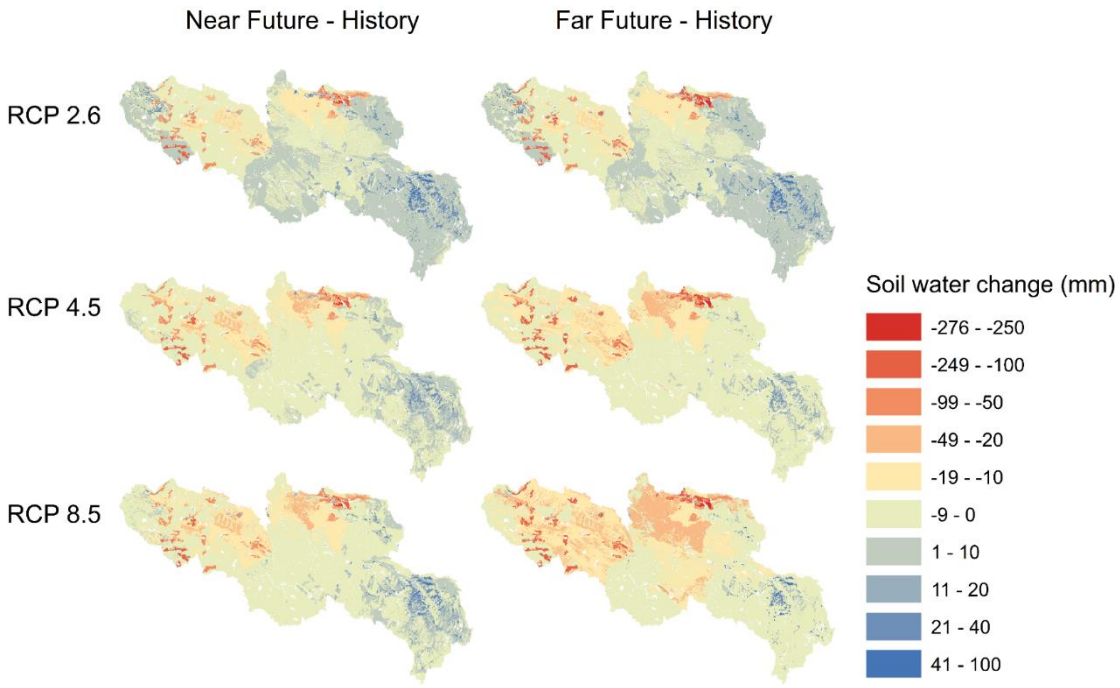

Figure S5. The difference of soil water between near future (2020–2059) and historical period, far future (2060–2099) and historical period under the RCP 2.6, 4.5, and 8.5.

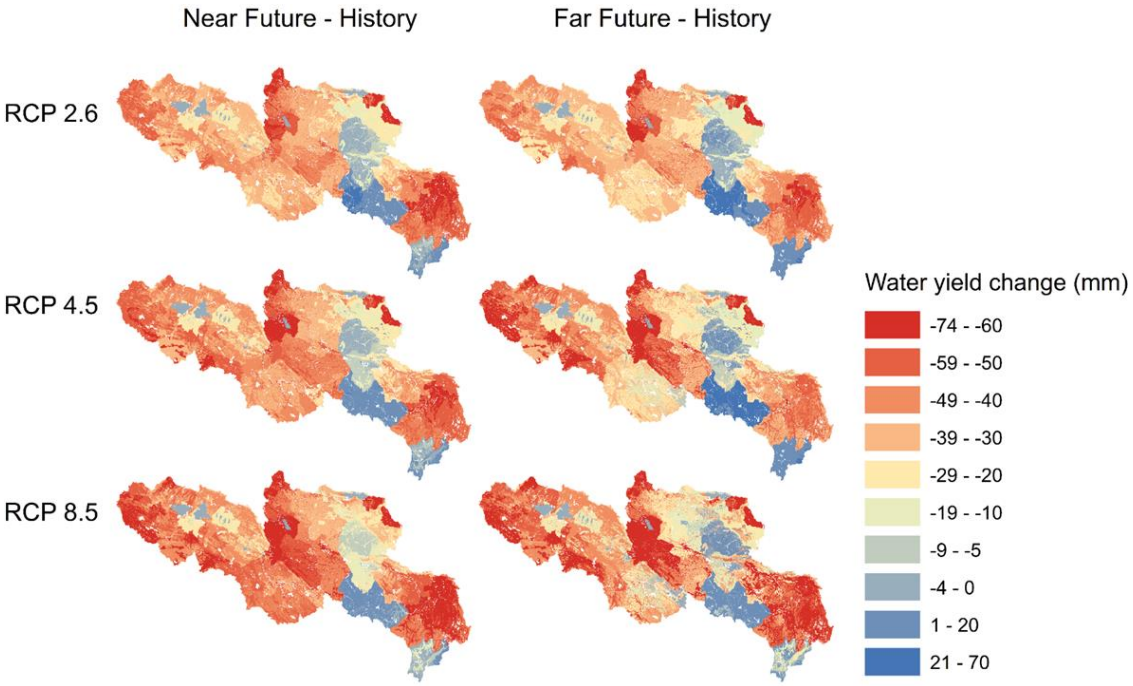

Figure S6. The difference of water yield between near future (2020–2059) and historical period, far future (2060–2099) and historical period under the RCP 2.6, 4.5, and 8.5.

Supplementary Files

This is a list of supplementary files associated with this preprint. Click to download.

- Supplementary0704.pdf